Homology Modeling Using Multiple Molecular Dynamics Simulations and Docking Studies of the Human Androgen Receptor Ligand Binding Domain Bound to Testosterone and Nonsteroidal Ligands†

Craig A. Marhefka,‡ Bob M. Moore II,‡ Thomas C. Bishop,§ Leonid Kirkovsky,‡ Arnab Mukherjee,‡ James T. Dalton,‡ and Duane D. Miller*,‡

Department of Pharmaceutical Sciences, College of Pharmacy, The University of Tennessee−Health Science Center, 847 Monroe Avenue, Room 327, Memphis, Tennessee 38163, and Center for Bioenvironmental Research at Tulane and Xavier Universities, Department of Environmental Health Science, Tulane University, 1430 Tulane Avenue SL-3, New Orleans, Louisiana 70112, Division of Basic Pharmaceutical Sciences, Xavier University of Louisiana

Received December 15, 2000

To facilitate the rational design of novel and more potent androgen receptor ligands, three-dimensional models for the human androgen receptor ligand binding domain bound to testosterone have been developed. These models of the androgen receptor were based on the crystal structure of the highly homologous human progesterone receptor ligand binding domain. The homology modeled androgen receptor was refined using unrestrained multiple molecular dynamics simulations in explicit solvent. Key H-bonding partners with the 17-hydroxy group and 3-keto group of testosterone are Asn705 and Thr877, and Gln711 and Arg752, respectively. These models show the presence of a unique unoccupied cavity within the androgen receptor binding pocket which may be valuable in the development of novel selective androgen receptor ligands. A qualitative analysis of amino acid mutations within the hAR binding pocket that affect ligand binding are consistent with these androgen receptor models. In addition to testosterone, the binding modes of several hydroxyflutamide-like nonsteroidal ligands for the androgen receptor are investigated using flexible docking with FlexX followed by refinement of the initial complexes with molecular dynamics simulations. These docking studies indicate that Asn705 is an important determinant in binding hydroxyflutamide and its derivatives by participating in H-bond interactions with the α-hydroxy moiety of these ligands. In addition, the nitro functionality mimics the 3-keto group of the natural ligand testosterone and is involved in H-bonding interactions with Gln711 and Arg752. From these docking studies, we suggest a mechanism for the enantioselective binding of chiral hydroxyflutamide derivatives and expand upon the previously reported structure−activity relationship for hydroxyflutamide and its derivatives.

Introduction

The androgen receptor (AR) is a member of the steroid/nuclear receptor superfamily of intracellular ligand-dependent transcription factors.[1,2] Its role is to modulate the biological effects of the endogenous androgens, testosterone (TES) and dihydrotestosterone (DHT). TES and DHT play numerous roles during male fetal and pubertal development. Androgens also maintain secondary sexual characteristics, such as muscle and bone mass, strength, fat distribution, and spermatogenesis.[3]

Members of the steroid/nuclear receptor superfamily consist of five structurally conserved domains.[1,2] On the basis of the crystal structures of the retinoic acid receptor (RAR-γ) and the retinoid-X receptor (RXR-α) and a sequence alignment analysis of other members of this superfamily,[4] it was proposed that all members of the steroid/nuclear receptor superfamily share a common ligand binding domain (LBD) fold. This idea is supported by the subsequent observation of this LBD fold in the thyroid receptor (TR-α_1),[5] human estrogen receptor (hER),[6,7] human progesterone receptor (HPR),[8] peroxisome proliferator-activated receptors (PPAR),[9,10] the vitamin D receptor,[11] and most recently the human androgen receptor (hAR).[12]

Synthetic androgens and antiandrogens have therapeutic value in the treatment of various androgen dependent conditions, from regulation of male fertility to prostate cancer. Steroidal AR agonists and antagonists are used clinically (e.g., cyproterone acetate); however, they suffer from a number of undesirable side effects including thrombosis, fluid retention, and loss of libido.[13] Nonsteroidal AR antagonists (e.g., hydroxyflutamide), which lack these undesirable side effects, have been developed and are currently used in the treatment of androgen-dependent prostate cancer.[13] To date there are no nonsteroidal androgens currently being used in the clinic. To aid in the design of novel and higher affinity nonsteroidal ligands, an understanding of the interactions between ligand and receptor at the molecular level would prove invaluable.

† This work was presented in part at the 218th National Meeting of the American Chemical Society, New Orleans, LA, August 22−26, 1999, Poster MEDI 218, and at the Keystone Symposia: Nuclear Receptors 2000, Steamboat Springs, CO, March 25−31, 2000, Poster 435.

* Phone: (901) 448-7529. Fax: (901) 448-6828. E-mail: dmiller@utmem.edu.

‡ The University of Tennessee−Health Science Center.

§ Center for Bioenvironmental Research at Tulane and Xavier Universities.

10.1021/jm0005353 CCC: $20.00
Published on Web 05/02/2001

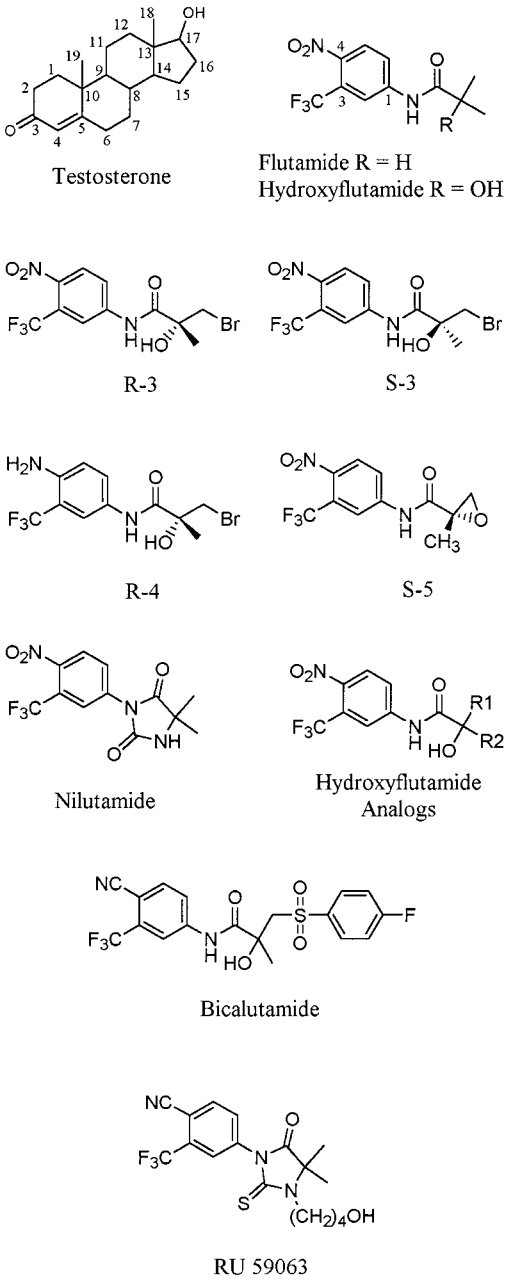

Figure 1. Structures of androgen receptor ligands used in this study.

Of the nonsteroidal ligands, hydroxyflutamide and its derivatives (e.g., bicalutamide and nilutamide) have been the most extensively studied. The commonly accepted structure−activity relationships (SAR) borne out of a broad base of structurally related compounds suggests (1) the importance for an electron-deficient aromatic ring, (2) the need for a strong H-bond donating group, and (3) a conformational preorganization such that the NH−CO−OH groups are coplanar.[14] In addition to these SAR elements, it has been shown that in bicalutamide (Figure 1), which contains a stereogenic center, the stereochemistry at this center is important in maximizing the affinity for the AR.[15]

In this work, we present three-dimensional models for the TES bound human AR (hAR) LBD, which were developed using unrestrained multiple molecular dynamics (MD) simulations in explicit solvent, and the crystal structure of the human PR LBD.[8] Qualitative analyses of natural mutations that affect the binding affinities of AR ligands are used to support the presented models. To further test the accuracy of these models, we have synthesized two new chiral derivatives of hydroxyflutamide (Figure 1; (*R*)-**3** and (*S*)-**3**) to study the binding modes and specific intermolecular determinants between these new ligands, hydroxyflutamide, nilutamide, and the hAR LBD. In addition, we synthesized two new ligands (Figure 1; (*R*)-**4** and (*S*)-**5**) to test the conclusions drawn from the docking studies. Preliminary comparisons with the recently determined crystal structure of the hAR LBD-R1881 complex are performed and show this method is an improvement over standard model refinement procedures.

Results and Discussion

hAR Model Building Approach. The hPR seemed well suited for the development of a hAR model, considering its high primary sequence homology to the hAR and the common tertiary fold among steroid receptors. We used the alignment reported by Williams et al.[8] to align the sequences of the hPR and hAR. The hAR (residues 669−918) is 56% identical to the hPR (residues 683−931). Furthermore, 32% of these residues are conservative mutations, giving an overall sequence homology of 87%. The absence of insertions or deletions within these sequences allowed for the direct mutation of the hPR residues to the corresponding residues of the hAR. As a result of this high homology and common LBD fold, the starting structure for our hAR model is expected to be near its native structure.

In the development of our hAR model, 10 independent 300 ps unrestrained MD simulations were performed in the presence of explicit solvent. Each simulation had different initial velocities, anticipating that each simulation should sample a unique minimum on the potential surface of the hAR native structure. This approach was applied by Caves et al.,[16] who showed that multiple, short (120 ps) MD simulations could sample the conformational space around the crystal structure of crambin more effectively than a single long simulation of 1 or 5 ns. In this study, the globally averaged structure obtained by averaging all 10 simulations together yielded a structure that was closer to the reference structure than any one of the 10 individually time averaged simulation structures. Here we apply this methodology to obtain final hAR LBD-TES complex global model structures.

To minimize errors introduced as a result of MD simulation conditions, we tested the MD conditions by performing a control simulation of the hPR LBD crystal structure. The results of these test simulations (see Supporting Information) are consistent with literature reports of similar simulations and comparisons between X-ray and NMR structures.[16−18]

hAR Model. The position of TES within the binding pocket in the hAR starting structure was identical to the position of progesterone (PGT) in the hPR crystal structure. After energy minimization of the initial hAR model, there were no potential H-bonding partners within 4 Å of the 17-hydroxyl group of TES. During the simulations, the 17-hydroxyl group of TES moved to H-bond with Thr877 and Asn705. As seen in Table 1, the H-bonds between the 17-hydroxyl group of TES,

Table 1. H-Bonds between TES and Binding Pocket Residues Expressed as Percent Occupancy during the Trajectories

	donor/acceptor					
model	GLN 711/ TES O3	GLN 711/ H_2O/ TES O3	ARG 752/ TES O3	ARG 752/ H_2O/ TES O3	THR 877/ TES O20	TES O20/ ASN 705
S1	79.94	na	6.76	na	98.24	99.24
S2	10.78	32.66	36.06	46.73	99.50	99.24
S3	47.75	20.00	7.75	5.75	41.75	74.00
S4	76.50	na	3.00	na	90.25	91.25
S5	30.50	37.75	2.00	26.75	59.00	71.25
S6	33.75	na	50.00	na	89.50	87.75
S7	34.50	na	50.50	na	96.50	94.75
S8	27.25	37.75	0.25	0.25	85.75	86.00
S9	17.50	10.75	18.50	26.00	94.50	94.00
S10	49.00	20.25	1.00	40.00	88.50	88.75

Gln705, and Thr877 were present for a substantial part of the simulation. The high stability of these H-bonds indicate that these H-bond interactions are significant in the binding of TES to the hAR. This is the same H-bonding pattern that is observed between metribolone (R1881) and the hAR LBD in the crystal structure.[12]

In our model of the hAR, Gln711 and Arg752 were involved in H-bonding with the 3-keto functionality of TES by both direct and water-mediated H-bonds. During the MD simulations, water molecules freely migrated in to and out of the crevice between helices 3 and 5 in close proximity to the 3-keto group of TES. This solvent filled crevice allows for increased conformational freedom of the Gln711 and Arg752 side chains. In six of the hAR simulations, this conformational freedom resulted in the intervention of a water molecule between the 3-keto group of TES and the Gln711 and Arg752 residues. The identity of the intervening water changed during the course of the simulation, indicating this H-bonding network is dynamic in nature. Table 1 shows the H-bond occupancies of Gln711 and Arg752 to TES, either directly or via a water molecule. This suggests the H-bonds to the 3-keto group of TES play a less significant role in the binding of TES to the hAR than the H-bonding interactions to the 17-hydroxyl of TES. Moreover, among the H-bonds to the 3-keto group, the Gln711 to TES H-bond appears to be more important than the Arg752 to TES H-bond. This observation is supported experimentally by the facts that no natural mutation of Gln711 has been identified and that the Arg752Gln mutation has only a slight effect on ligand binding.[19] In addition, if the 3-keto of DHT is reduced to the corresponding alcohol, there is an 8−12-fold loss in binding to the AR. If the 17-hydroxy group of DHT is oxidized to the corresponding ketone, there is a 60−120-fold loss in binding to the AR, adding further support to this idea.[20]

Two final hAR LBD models, a direct H-bonding model, G1, and a water-mediated model, G2, were developed to account for the two observed H-bonding patterns to the 3-keto group of TES (Figures 2 and 3). The two hAR models and the time averaged hPR structure had greater than 98% of their residues in allowed regions of the Ramachandran plots and 100% stereochemical correctness when checked with PROCHECK.[23] The direct H-bonding model, G1, more closely represents the observed H-bonding patterns to the hPR and hER crystal structures, thus we chose to use this model in the subsequent analysis and docking.

A unique feature in the hAR LBD model is the presence of an unoccupied cavity within the binding pocket (Figure 4) on the α side of the steroid plane, beneath and adjacent to carbon 15 of TES. The volumes of the hAR binding pocket and TES, as defined by the molecular surface, are 666 Å^3 and 281 Å^3, respectively. Both the hPR and hER crystal structures have smaller cavity volumes, 603 Å^3 and 559 Å^3, with ligand volumes of 309 Å^3 and 249 Å^3, respectively. Two amino acid differences between the hAR and hPR in this region may be responsible for the difference in pocket volumes. In the hAR, the smaller, more flexible Met780 takes the place of Phe794 of the hPR, and the more polar Gln783 takes the place of Leu797. A result of the Leu797 to Gln783 change is the amide portion of Gln783 prefers to be at the solvent exposed surface of the structure, leaving only the β- and γ-methylene carbons for hydrophobic interactions with the interior. In the hPR, the whole side chain of Leu797 buries itself in the interior of the structure, filling this space in the binding pocket.[8] The flexibility of Met780 in the hAR results in the volumes of the ligand binding pockets in each simulation structure being different. The average pocket volume was 646 ± 32 Å^3 with a range of 579 Å^3 to 679 Å^3. In the simulation that gave the pocket volume of 579 Å^3, Met780 closes off the pocket while in the others it does not. The root-mean-squared fluctuation (RMSF) of Met780 is 1.3 Å, corresponding to a crystallographic *B*-factor of 45. The average RMSF for all the residues that make up this unoccupied pocket is 1.1 Å (*B*-factor of 31). The average *B*-factor for the corresponding residues in the hPR is 27, while Phe794 has a *B*-factor of 43. Although Phe794 in the hPR also has significant motion as indicated by the *B*-factor, this residue is three carbons larger and less flexible then Met, precluding a similar pocket in the hPR. Considering the high mobility of these residues during the simulations and the variation in the hAR binding pocket volume for each simulation structure, we concluded that this pocket is not an artifact resulting from reduced conformational sampling during the simulations.

We analyzed the effects of binding pocket residue mutations on the affinity of hAR ligands (Table 2). Analyses of many of these mutations in the G1 model yield the same conclusions drawn by Matias et al. in the analysis of the hAR-R1881 crystal structure.[12] However, some mutations were not discussed by Matias et al. The Trp741Arg mutation results in the placement of a charged residue in a hydrophobic environment, likely causing a destabilization of the receptor itself or the ligand bound complex. Our model suggests the Ala748Asp mutation is tolerated with little effect on ligand binding because the charged side chain of Asp can be accommodated in the solvated crevice between helices 3 and 5. The Met787Val substitution alone would cause a moderate increase in the size of the hAR binding pocket; however, because it is adjacent to the unoccupied cavity, the impact on the binding pocket size is more substantial. The Val889Met mutation is located in the flexible loop between helices 11 and 12, accommodating the added size. Finally, the Met895Thr mutation increases the volume of the binding pocket, decreasing the hydrophobic interactions with TES.

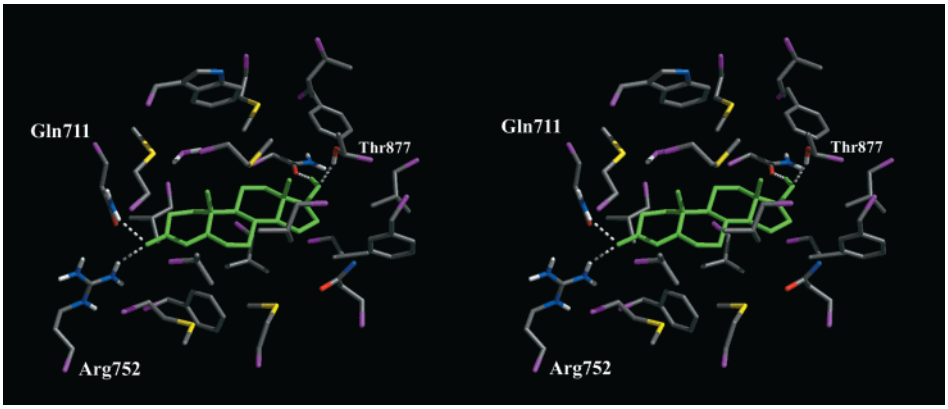

Figure 2. Stereoview of the G1 model ligand binding pocket. C^{α} are colored violet. Figure generated with MidasPlus.[21,22]

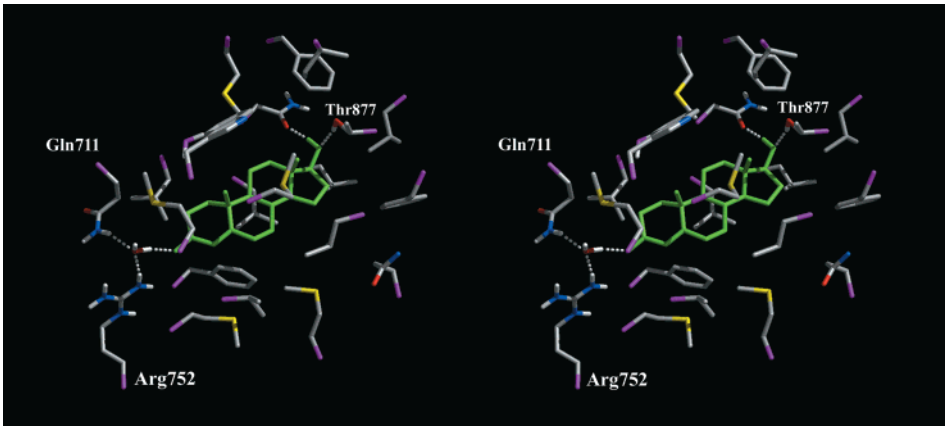

Figure 3. Stereoview of the G2 model ligand binding pocket. C^{α} are colored violet. Figure generated with MidasPlus.[21,22]

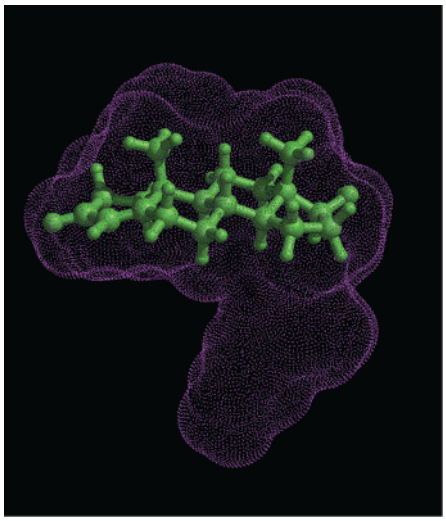

Figure 4. Solvent accessible surface area (1.4 Å probe) of the G1 model's binding pocket. Figure generated with MidasPlus.[21]

Table 2. hAR Binding Pocket Mutations That Affect Ligand Binding

mutation	location	effect on K_d	consistent with model
Asn705Ser	beginning of H3	nd[a]	√
Leu707Arg	middle of H3	nd[b]	√
Trp741Arg	beginning of H5	nd[c]	√
Met742Ile	beginning of H5	3−5-fold ↑[d,e]	√
Met742Val	beginning of H5	nd[f]	√
Met745Thr	middle of H5	nd[f]	√
Ala748Asp	middle of H3	1.8-fold ↑[c]	√
Arg752Gln	end of H5	2-fold ↑[g]	√
Phe764Leu	S1 Sheet	1.8-fold ↑[c]	√
Met787Val	middle of H7	> 1000-fold ↑[h]	√
Thr877Ala	end of H5	1.2-fold ↑ in RBA[i]	√
Val889Met	H11-H12 Loop	1.2-fold ↑[g,j]	√
Met895Thr	beginning of H12	6-fold ↑[k]	√

[a] Experimental data from De Bellis et al.[24] nd = not detectable. [b] Experimental data from Lumbrosso et al.[25] [c] Experimental data from Marcelli et al.[26] [d] Experimental data from Bevan et al.[27] [e] Experimental data from Batch et al.[28] [f] Experimental data from Ris-Stalpers et al.[29] [g] Experimental data from Langley et al.[19] [h] Experimental data from Nakao et al.[30] [i] Experimental data from Veldscholte et al.[31] [j] Experimental data from DeBellis et al.[32] [k] Experimental data from Lundberg et al.[33]

Comparison with the hAR-R1881 Crystal Structure. During the preparation of this manuscript, the X-ray crystal structure for the hAR LDB and hPR LBD bound to R1881 was described at a resolution of 2.4 and 2.8 Å, respectively.[12] Matias et al. report a main chain root-mean-squared deviation (RMSD) of 1.22 Å for the hAR LDB-R1881 complex when compared to the hPR LBD-PGT complex, where the G1 model has an RMSD of 1.55 Å when compared to the hPR LBD-PGT complex. The G1 model has an RMSD of 1.1 Å in the helical element C^{α} atoms and 1.2 Å for all main chain atoms when compared to the hAR-R1881 crystal structure. The binding pocket residues had main chain and side chain RMSDs of 0.76 and 1.33 Å, respectively, when compared to the same residues in the hAR-R1881 complex. The residues involved in H-bonding TES and R1881 (Asn705, Gln711, Arg752, and Thr877) had main chain and side chain RMSDs of 0.65 and 0.97 Å, respectively.

There are, as one might expect, some differences between our models and the crystal structure. Among these is the presence of a H-bond between Gln711 and the 3-keto group of TES in our model which is not

Scheme 1. Chiral Synthesis of AR Ligands[a]

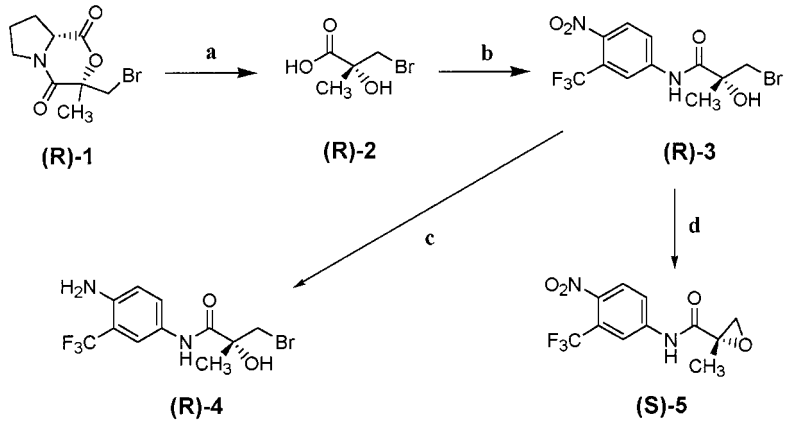

[a] Reagents and conditions: (a) 24% HBr, reflux; (b) anhydrous DMA, $SOCl_2$, −10 to −15 °C, then 5-amino-2-nitrobenzotrifluoride; (c) $SnCl_2$/MeOH, 0 °C → rt; (d) acetone/K_2CO_3.

present in the hAR LBD-R1881 complex crystal structure.[12] This difference in the H-bonding pattern likely results from the different ligands studied in these two cases. Different H-bond patterns are seen when the hPR is bound to PGT or R1881. When the hPR is bound by PGT, the 3-keto group of PGT is H-bonding with both Arg766 and Gln725. On the other hand, when the hPR is bound by R1881, two different H-bonding patterns are observed. One molecule of the hPR-R1881 complex shows R1881 H-bonding with both Arg766 and Gln725, while the other molecule in the crystal structure R1881 is H-bonding to Arg766 alone. This observation suggests that the H-bonding patterns vary depending on the ligand bound to the receptor. The hAR like the hPR may have different H-bonding patterns to the 3-keto group of R1881, but experimental conditions precluded both from being observed in the hAR-R1881 crystal structure. The hAR may also have different H-bonding patterns for different ligands.

Another possible difference between our models and the X-ray structure is the presence of the unoccupied pocket below TES C15. Matias et al. do not explicitly discuss the presence or absence this pocket; however, the main chain and side chain RMSDs for the residues that comprise this pocket are 0.87 and 1.66 Å, respectively. Two residues that make up this pocket, Met780 and Gln783, have significant deviation from the hAR-R1881 crystal structure. In the crystal structure Gln783 is interacting with solvent more than is observed in the model, and the orientation of the amide group is opposite of that in our G1 model. This difference would make the unoccupied pocket slightly larger than seen in our model. Although the orientation and positioning of the Gln783 side chain is different in the final G1 model, its position and orientation in a number of the simulation structures is similar to that found in the crystal structure. In addition, the *B*-factor of this residue is higher than the average for the residues that comprise this unoccupied pocket in both the crystal structure and the model, showing that Gln783 in the model has conformational freedom similar to that observed in the crystal structure. Met780 is located in the loop between helices 6 and 7, which has different conformations in the crystal structure and the G1 model. Again, in both the crystal structure and the model, the *B*-factor for Met780 is well above the average for the residues that comprise this unoccupied volume in the binding site. This suggests the environment neighboring Met780 is similar in both structures. All other residues in this pocket have similar side chain conformations whose deviations are within rotational barriers that are crossed and observed during the simulations.

We show in this paper that the method for homology model refinement applied here has benefits over methods that depend on no energy refinement or solely energy minimization of a mutated protein. This is highlighted by a homology model developed by the same group that solved the crystal structure.[12] In the refinement of this homology model, the protein was solvated with a shell and minimized while holding the C^{α} to their initial positions with a restraining potential.[34] This method resulted in an RMSD of 1.09 Å for C^{α} in the helical elements where our G1 model had an RMSD of 1.1 Å in the helical element C^{α} atoms. Another example is a recent homology model by Poujol et al.[35] Their model was also based on the hPR crystal structure; however, energy minimization of only the amino acid side chains and R1881 ligand was performed. This model inaccurately predicts the H-bonding situation between the 17-hydroxyl group of R1881 and the hAR, showing no H-bonding between Thr877 and R1881. In addition to resulting in a more accurate model, the method for homology modeling presented here gives some insights to the dynamic behavior of the protein ligand complex.

Chemistry and Binding. Scheme 1 shows the synthesis of (*R*)-4-nitro-3-trifluoromethyl-bromoanilide ((*R*)-**3**) with the *S* isomer being synthesized in the same manner. The (*R*)-**1** or (*S*)-**1** bromolactone was synthesized using the method of Kirkovsky et al.[36] The chiral bromolactone was hydrolyzed using HBr, in contrast to the previously reported use of HCl, to avoid obtaining a mixture of both brominated and chlorinated acids as was the case reported by Kirkovsky et al. The bromo acids were then converted to their acid chlorides in situ at −10 to −15 °C in DMA with thionyl chloride. A solution of 5-amino-2-nitrobenzotrifluoride in DMA was then added and stirred at room temperature overnight, yielding the final (*R*)-**3** or (*S*)-**3** products. The (*R*)-4-amino-3-trifluoromethyl-bromoanilide was obtained by the reduction of (*R*)-**3** with tin chloride in methanol at room temperature. Compound (*R*)-**3** was treated with

Table 3. Binding Affinity for Novel HAR Ligands

ligand	K_i (nM)
(*R*)-**3**	0.3 ± 0.1 nM
(*S*)-**3**	16.5 ± 1.2 nM
(*R*)-**4**	80.9 ± 0.5 nM
(*S*)-**5**	no binding

Table 4. Derived Small Molecule AMBER Torsion Parameters

torsion	bond paths	$V_n/2$	phase	n
N−C−CT−OH	1	0.15	180	−3
N−C−CT−OH	1	1.20	180	2
X−N−CA−X	4	1.12	180	−3
X−N−CA−X	4	2.43	180	−2
X−N−CA−X	4	5.75	180	1

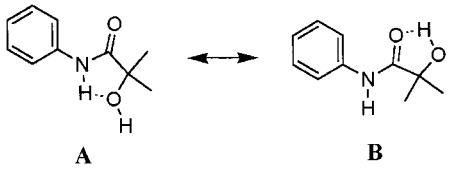

Figure 5. Intramolecular H-bonding conformations found in hydroxyflutamide type AR ligands demonstrated by the model compound used to develop the O=C−C−O torsion parameter.

K_2CO_3 in acetone to form the epoxide (*S*)-**5** by intramolecular SN_2 elimination. Note that the geometrical configuration of the epoxide remains the same while the absolute configuration changes. Table 3 lists the binding affinities for these new AR ligands.

Parameter Development for the Nonsteroidal Ligands. The standard AMBER force field[37,38] lacks several parameters that are necessary for the treatment of our small molecule ligands. Where appropriate, bond, angle, and nonbonded parameters for the nonsteroidal ligands were transferred by chemical analogy from the standard set of AMBER parameters. Partial atomic charges for the ligands and model compounds were developed using the RESP program of the AMBER 5 to fit HF/6-31G* derived electrostatic potential grids to atom centers in a two-stage process.[39,40]

Of special interest to this study is the α-hydroxy amide moiety of hydroxyflutamide and its chiral derivatives studied here. Previous physicochemical studies of hydroxyflutamide and derivatives of hydroxyflutamide showed that the intramolecular H-bonding of these compounds prefers one conformation, **A**, over the other, **B** (Figure 5).[14] To accurately represent this intramolecular H-bonding interaction, the energy profile about the O=C−C−O torsion of a model compound, 2-hydroxy-2-methyl-*N*-phenyl-propionamide (Figure 5), was calculated in 10° increments at the HF/6-31G* level of theory using the scan feature in Gaussian 98[41] with geometry optimization at each increment. This unsubstituted model compound was chosen for computational efficiency and is a valid selection based on experimental data which show that substitutions on the aromatic ring have no effect on the **A** to **B** equilibrium.[14] Previous ab initio calculations at a lower level of theory on a less representative model compound predicted an **A** to **B** energy difference of 1.5 kcal/mol.[14] Here, we show this difference to be 1.9 kcal/mol.

A new program, *parmscan*,[42] was used to derive the AMBER torsional parameters (Table 4) for the α-hydroxy amide moiety. Five points along the ab initio

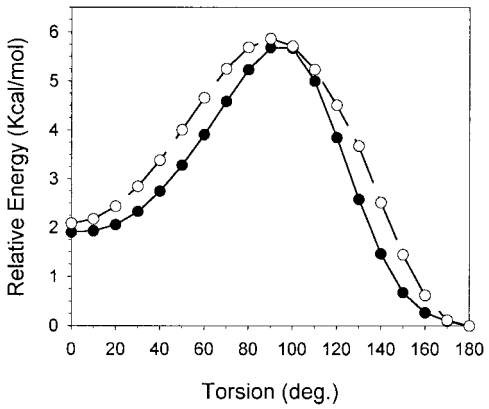

Figure 6. Closed circles: ab initio energy profile used to develop the O=C−C−O torsion of model compound. Open circles: AMBER calculated energy profile, including parameters developed with *parmscan*, for the O=C−C−O torsion, of the model compound.

calculated energy surface (Figure 6) were selected for parameter development (0, 60, 100, 160, and 180), giving four energy difference pairs that were used as input data for *parmscan*. Two specific torsion parameters for N−C−C−O (V_3 and V_2) were found that sufficiently reproduce the ab initio data with an average absolute error (AAE) for these energy pairs of 0.3232. These specific torsion parameters were then used to calculate an AMBER energy profile for the model compound, resulting in a very good correlation (r^2 of 0.9701) between the ab initio and AMBER calculated energy profiles (Figure 6).

We also developed torsion parameters for the aromatic amide portion of hydroxyflutamide (C−C−N−H and C−C−N−C) using acetanilide as a model compound. Here HF/6-31G* level ab initio calculations were performed at 0°, 45°, and 90° as well as the AMBER calculated energy profile with the force constant for this torsion set to zero. The difference curve (e.g., ab initio energy at 0° minus AMBER energy at 0°) was fit to the Fourier series of the Cornel et al.[38] force field with a regression program to give general AMBER torsion parameters (Table 4). These general torsion parameters were then used to calculate an AMBER energy profile for acetanilide. The minima of the AMBER calculate profile was located at 35°. Since we only calculated the ab initio energies at three data points and developed the AMBER torsion parameters on this limited data set, we felt this may not have been sufficient for accurate parameter development. We, therefore, went back and calculated the HF/6-31G* energies at 25° and 35° to check if the AMBER calculated minima fell in the correct range (Figure 7). The energy minima for this expanded ab initio data was also 35°. The AAE for these five data points was 0.1409. In this case, torsion parameter development on three data points was sufficient to accurately reproduce the ab initio energy profile ($r^2 = 0.996$).

Binding Model for Hydroxyflutamide, (*R*)-3, and (*S*)-3. Hydroxyflutamide, (*R*)-**3**, and (*S*)-**3** had highly similar docking with regard to the placement of the electron deficient aromatic ring (Figure 8). In all of these compounds, the nitro group is positioned such that it may participate in H-bonding interactions with Gln711 and Arg752 in a manner analogous to that of the 3-keto

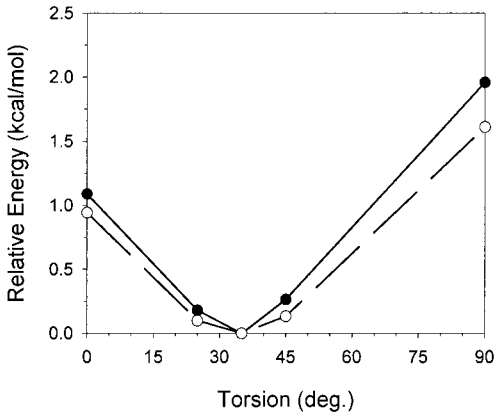

Figure 7. Closed circles: ab initio calculated energy profile used to develop the X−C−N−X torsion of acetanilide. Open circles: AMBER calculated energy profile, including developed parameters for the X−C−N−X torsion, of acetanilide.

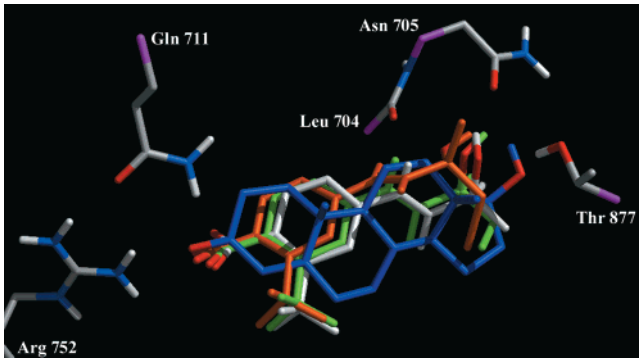

Figure 8. Hydroxyflutamide (white), (*R*)-**3** (green), and (*S*)-**3** (orange) superimposed on testosterone (blue) within the hAR binding site. Oxygen atoms of the ligands are red, and backbone α-carbons are magenta. Figure generated with MidasPlus.[21,22]

group of TES. Here, as is the case with TES, the H-bonding interactions with Gln711 was 3.5 to 4 times more predominant during the simulations than the H-bonding interactions with Arg752. The trifluoromethyl group of the aromatic ring lies in a hydrophobic region adjacent to and in the plane of atoms 4, 5, and 6 of TES (Figure 9).

The hydroxyl group α to the carbonyl in hydroxyflutamide, (*R*)-**3**, and (*S*)-**3** is positioned such that it H-bonds with Asn705. Hydroxyflutamide and (*R*)-**3** also show H-bonding to Thr877, while the configuration about the chiral carbon of (*S*)-**3** causes this hydroxyl group to be positioned 3.6 Å from Thr877 and places the methyl group between itself and Thr877, preventing any H-bond interactions from occurring.

(*R*)-**3** and (*S*)-**3** differ from hydroxyflutamide in that bromine replaces hydrogen on one of the methyl groups conferring chirality to the ligand. In (*R*)-**3**, the bromine occupies the hydrophobic pocket that the 18-methyl group of TES occupies while the methylene carbon fills the space where the 16 and 17 carbons of TES would be in the hAR-TES complex (Figure 8). The methyl group of (*R*)-**3** fills a small hydrophobic pocket below the plane of TES at C17 (Figure 9). The existence of this small hydrophobic pocket is supported experimentally by the higher affinity of 7α-fluoro-17α-methyl-DHT over 7α-fluoro-DHT for the AR.[43] The bromine in (*S*)-**3**, however, occupies the space of carbons 15 and 16 in TES with the methylene group occupying the space of the 18-methyl group (Figure 8). Due to the inversion of absolute configuration, the methyl group of (*S*)-**3** is oriented such that it has steric interaction with Met895 on helix 12 of the hAR LBD, causing a change in the side chain conformation that could destabilize the ligand bound conformation of helix 12 resulting in a faster unbinding event.

The amide proton of both (*R*)-**3** and (*S*)-**3** also form a weak H-bond with the backbone oxygen of Leu704. This additional H-bond along with increased hydrophobic interactions with the hAR accounts for the higher affinity of both (*R*)-**3** and (*S*)-**3** over hydroxyflutamide. The enantioselectivity observed between (*R*)-**3** and (*S*)-**3** is a result of an additional H-bond between (*R*)-**3** and Thr877, in addition to the absence of a steric interaction of the methyl group as is the case with (*S*)-**3**.

Binding Model for Nilutamide. The initial hAR-nilutamide complex obtained after the FlexX docking was similar to those obtained for (*R*)-**3**, (*S*)-**3**, and hydroxyflutamide. After the refinement protocol, nilutamide shifted approximately 1 Å toward Thr877 to allow the amide proton of the hydantoin ring to H-bond with Thr877 (Figure 10). The initial FlexX placement of nilutamide had this amide proton in a position to H-bond with Asn705; however, there were steric interactions between the hydantoin ring and amino acids within the AR binding site. This steric conflict in the initial complex was a result of the van der Waals (VDW) overlap allowances used in the docking algorithm. As a result of the translation toward Thr877, the aromatic nitro group only forms direct H-bonds to Gln711. A water molecule enters this end of the binding pocket, through the solvent accessible cleft between helix 3 and helix 5, and positions itself between the nitro group and Arg752, allowing it to act as a H-bond mediator between these groups. The trifluoromethyl group of nilutamide binds in the same hydrophobic pocket as is observed with hydroxyflutamide, (*R*)-**3**, and (*S*)-**3**. One of the methyl groups on the hydantoin ring binds in the hydrophobic pocket below the 17 carbon of TES, and the other occupies the space of the 16 carbon of TES.

Structure−Activity Relationship. We suggest a modification to the first point of the accepted SAR, the need for an electron deficient aromatic ring. Instead of a need for an electron withdrawing substituent at the 3 position of the aromatic ring (e.g., hydroxyflutamide), we propose that a hydrophobic group at this position is important for enhanced binding to the AR. It has been generally accepted that the electron withdrawing groups can make the amide proton more acidic thereby enhancing the A to B equilibrium toward the A conformation (Figure 5).[44] This, however, has been shown not to be the case. A separate study by the same group showed that there is no change in the intramolecular H-bonding conformation, 100% A, of the α-hydroxy amide moiety upon changing the trifluoromethyl substituent to hydrogen or both ring substituents of hydroxyflutamide to hydrogen.[14] This demonstrates that the electronic effects of substituents at this position have a negligible effect on the A to B equilibrium of the α-hydroxy amide moiety. There is, however, a trend toward higher affinity and efficacy with an increase in the Hansch π values for the substituents at the 3 position. For example, there

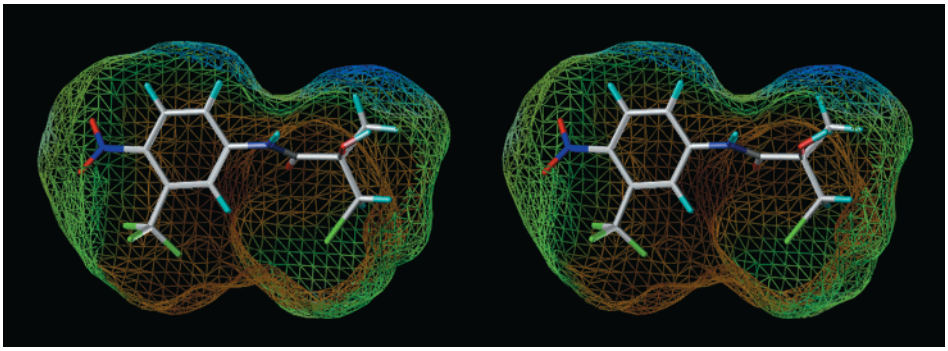

Figure 9. Stereoview of the accessible surface area (1.4 Å probe) of the binding pocket with (*R*)-**3** bound.

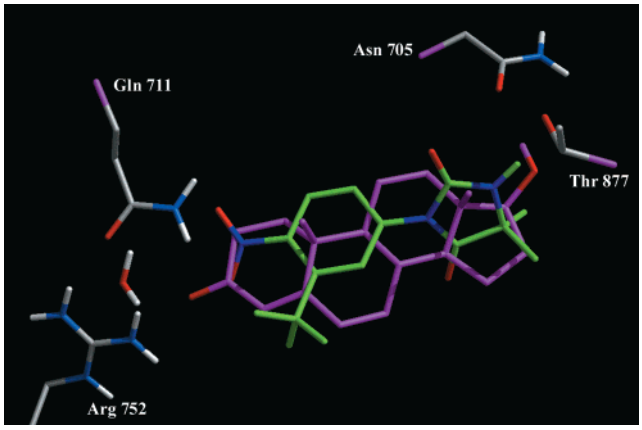

Figure 10. Nilutamide (green) superimposed on testosterone (magenta) within the hAR binding site. Oxygen atoms of the ligands are red, nitrogen atoms of nilutamide are blue, and backbone α-carbons are magenta. Figure generated with MidasPlus.[21,22]

is a 3-fold increase in affinity when the trifluoromethyl group of RU 59063 (Figure 1) is changed to an iodo group.[45] Also, when the three position of biclautamide derivatives are substituted by hydrogen, methyl, chloro, or trifluoromethyl, the antiandrogenic efficacy increases according to hydrophobicity of the substituent.[46] This increase in efficacy with hydrophobicity may be explained by the presence of the hydrophobic region within the binding pocket as discussed above. This hydrophobic region is also found in the hPR with the same amino acids composing the pocket with the exception of a Leu in the place of Met749. The presence of this region in both the hPR and hAR is supported by the fact that both these receptors have affinity for various hydroxyflutamide derivatives.[47] The presence of an H-bond acceptor (i.e., nitro or cyano groups[44−48]) at the 4 position of the aromatic ring that can interact with Gln711 and Arg752 significantly enhances the AR binding of this class of ligands. To probe this concept, the amino analogue of (*R*)-**3** was synthesized, (*R*)-**4**, and shows an affinity for the hAR that is 270-fold lower than (*R*)-**3**. Analogously, the 4-amino derivative of nilutamide has an affinity significantly lower than the nitro containing nilutamide.[49]

The need for a strong H-bond donor in the ligand is critical for the H-bonding interactions between the ligand and Asn705 and/or the ligand and Thr877. The removal of this H-bond donor results in a complete loss of ligand binding to the AR as is seen when flutamide is compared to hydroxyflutamide.[14] To further highlight this, we synthesized the epoxide, (*S*)-**5**, which shows no binding affinity for the hAR. The importance of the Asn705 in binding hydroxyflutamide and bicalutamide has been demonstrated by a site directed point mutant of Asn705 to Ala, resulting in a complete inability of these ligands to act as antagonists.[35] In the case of nilutamide, however, this SAR is not as strict. If the proton bearing nitrogen is replaced by oxygen, this compound still retains substantial antiandrogenic activity.[49] Thr877 can act as both a H-bond acceptor and donor; thus for the case of the oxygen containing derivative of nilutamide, Thr877 can act as an H-bond donor instead of an H-bond acceptor which is the case for nilutamide.

Studies aimed at the replacement of the amide group suggested that the amide moiety is critical for maintaining high affinity binding but probably does not interact directly with the AR itself.[44] In this study the amide proton of the chiral brominated derivatives is involved in direct H-bond interactions with a backbone carbonyl group. This observation identifies the structural basis for the specific role of this amide proton in hydroxyflutamide derivatives.

The preorganization of the NH−CO−C−OH torsion corresponding to conformation A in Figure 2 may be important in that it is this conformation that is seen in the docked ligands. This preorganization may increase the binding affinity of these ligands for the AR because the predominant conformation observed in solution is the same as the bound conformation. Thus there is no additional entropic cost for ligand reorganization before binding the receptor.

In addition to these accepted structure−activity relationships, we can rationalize the high affinity and efficacy for a number of hydroxyflutamide derivatives upon the replacement of one or both of the methyl groups of with a variety of substituents. The nature of the substituents range from simple alkyl and aryl groups to heteroaromatic rings.[44,46,47,50,51] For the modification in an analogous position to that of the bromine in (*R*)-**3**, we expect that these moderate to large substituents have access to and can be accommodated by the pocket below the C15 of TES. This is supported by a series of compounds where R1 (Figure 1, hydroxyflutamide analogs) is methyl or trifluoromethyl and R2 is phenyl, *p*-nitrophenyl, *p*-cyanophenyl, benzyl, *p*-fluorobenzyl, *n*-butyl, or ethyl. These compounds retain a similar binding affinity to the parent compound[44,51] and show increased androgenic activity over the parent compound.[47]

Conclusions

In an effort to understand the molecular interactions between the hAR and TES, we developed three-dimensional models for the hAR LBD bound to testosterone based on the hPR LBD progesterone complex crystal structure. From preliminary comparisons with the hAR-R1881 complex crystal structure, this method of homology model refinement seems superior to simple energy based refinement methods. These models indicate that Asn705 and Thr877 form stable H-bonds with the 17-hydroxy group of TES. At the opposite end of the pocket, Gln711 and Arg752 form more dynamic H-bonds with the 3-keto group of testosterone, which can be either direct or water mediated. Binding pocket mutations which affect ligand binding to the hAR are consistent with our models. We have presented models for the binding modes of several nonsteroidal ligands for the hAR. These models were used to investigate the structural basis of the currently accepted structure−activity relationships as well as to modify the SAR to account for both experimental and modeling observations. We suggest that the aromatic ring for compounds within this class of nonsteroidal ligands need not necessarily be electron deficient but rather have a H-bond acceptor in the 4 position to mimic the 3-keto group of testosterone and a hydrophobic group at the 3 position to take advantage of the hydrophobic region within the AR ligand binding site. The strong H-bond donor within the ligand is required for the formation of H-bonding interactions with Asn705 and/or Thr877 of the AR. Enantioselective binding of bicalutamide and other chiral hydroxyflutamide derivatives results from the positioning of the methyl group such that the hydroxyl group is prevented from forming a H-bond with Thr877 in addition to having steric interaction with Met895 on helix 12 reducing the AR binding.

Experimental Section

Model Building and Refinment. All simulations were performed using the SANDER program of the AMBER 5[37] suite using the Cornell et al. force field and the "param96" parameter set.[38] TES and PGT were assigned existing AMBER atom types. Partial atomic charges were developed using the RESP program to fit HF/6-31G* derived electrostatic potential grids to atom centers in a two-stage process.[39,40] The crystal structure for the hPR LBD (PDB ID 1A28) served as the basis for our hAR model.[8] Mutation of the side chains of the hPR to the corresponding side chains in the hAR was performed in the Biopolymer module of Sybyl 6.5.[52] The "mutate monomer" function of Biopolymer places the new amino acid side chains using the coordinates from the existing side chains such that the β-carbon of the new side chain assumes the coordinates of the old side chain. If the new side chain has more atoms than the old side chain, the conformation for the remaining atoms are obtained from a database of low energy conformations. In this case, the mutated side chains were manually positioned to minimize steric interactions with adjacent residues. After all mutations were complete, a series of minimizations were performed to relax the structure. The minimizations started with the binding pocket side chains and worked outward in concentric spheres until all the side chains were unconstrained. This was followed by a final minimization of the entire protein. The LBDs were immersed into a box of TIP3P waters using the LEaP utility of AMBER 5. The hPR and hAR systems contained 8582 and 9058 water molecules, respectively. Equilibration and warming of the systems was similar to the method of Fox et al.[53] Briefly, the solvent was minimized to an RMS gradient of 0.5 kcal/Å followed by 12 ps of MD at 150° K, while holding the protein rigid with a harmonic potential of 1000 kcal/Å^2. The system was then subjected to six minimizations slowly lowering the restraining potential on the protein atoms. Finally, two completely unrestrained MD simulations were performed at 100 and 200 K for 6 and 9 ps, respectively. These systems were then used for production simulations. The MD time step was 1.5 fs using SHAKE[54] to constrain bonds to hydrogen. An 8 Å residue charge group based cutoff for nonbonded interactions was used, and the nonbonded pairlist was updated every 15 steps. This cutoff was chosen to reduce the computational time involved due to the size of the systems (approximately 40 000 atoms) and larger cutoffs (i.e., 14 Å) or inclusion of all solute−solute interactions do not demonstrate a benefit over shorter cutoff values.[53,55] The system was maintained at 300 K , 1 atm constant pressure using periodic boundary conditions, and a dielectric constant of 1.

Time averaged structures were generated by time averaging the individual simulations from the point a stable trajectory was obtained through the end of the simulation. The final hAR models were obtained by averaging the appropriate simulation structures together. Averaged structures were minimized with 100 steps of steepest descent followed by conjugate gradient minimization to an RMS gradient of 0.01 kcal/Å. In the structures that contained a H-bond mediating water, a 5 kcal/Å^2 distance restraint was included in the minimization to position the water as it was observed during the simulations.

RMSD, RMSF, R_{gyr}, and H-bond interactions of the trajectories and time averaged structures were performed using the CARNAL program of the AMBER suite. The dms program from MidasPlus[21] was used to calculate the solvent accessible surface areas. Pocket volume calculations were performed with MOLCAD[52] using a grid spacing of 0.18 Å and a probe radius of 1.4 Å.

Chemistry. Melting points were determined on a Thomas-Hoover capillary melting point apparatus and are uncorrected. Proton and carbon-13 magnetic resonance spectra were obtained on a Bruker ARX 300 spectrometer (300 and 75 MHz for ^{1}H and ^{13}C, respectively). Mass spectral data was collected on a Bruker ESQUIRE electrospray/ion trap instrument. Elemental analyses were performed by Atlantic Microlab Inc., Norcross, GA. Specific rotations were recorded on Autopol III Automatic Polarimeter (Rudolph Research, Fairfield, NJ) in 1 dm sample tube with use of sodium D-line at ambient temperature. Routine thin-layer chromatography (TLC) was performed on silica gel aluminum plates (Whatman Ltd., Maidstone, Kent, England). Flash chromatography was performed on silica gel (Merck, grade 60, 230−400 mesh, 60 Å).

(2*R*)-3-Bromo-2-hydroxy-2-methylpropanoic acid (*R*-2). Bromoacid (*R*)-**2** was prepared by acid-catalyzed hydrolysis of bromolactone (*R*)-**1** (66.35 g, 253 mmol) in 650 mL of refluxing 24% HBr for 1.5 h. The solution was cooled and extracted with six 500 mL portions of ether. The combined ether extracts were dried ($MgSO_4$) and evaporated to dryness. The resulting solids were recrystallized from toluene yielding 39 g of (*R*)-**2**. (84%): mp 113.5−114.5 °C; $[\alpha]_D^{25}$ +10.5 (c = 2.6, MeOH); ^{1}H NMR (DMSO-d_6) δ 3.63 (d, J = 10.1 Hz, 1H, CH(1)), 3.52 (d, J = 10.1 Hz, 1H, CH(2)), 1.35 (s, 3H, Me).

(2*S*)-3-Bromo-2-hydroxy-2-methylpropanoic Acid (*S*-2). Bromoacid (*S*)-**2** was prepared from 45 g (246 mmol) of bromolactone (*S*)-**1** using the same method as the corresponding *R* isomer yielding 36 g (80%): mp 113−114 °C; $[\alpha]_D^{25}$ −11.3 (c = 2.6, MeOH); ^{1}H NMR (DMSO-d_6) δ 3.63 (d, J = 10.1 Hz, 1H, CH(1)), 3.52 (d, J = 10.1 Hz, 1H, CH(2)), 1.35 (s, 3H, Me).

***N*-[4-Nitro-3-(trifluoromethyl)phenyl]-(2*R*)-3-bromo-2-hydroxy-2-methylpropan Amide (*R*-3)**. Bromoanilide (*R*)-**3** was prepared using the general procedure of Tucker et al.,[56] yielding a mixture of product and starting aniline. In general, thionyl chloride (8.6 g, 72 mmol) was added dropwise to a cooled solution of (*R*)-**2** (11.0 g, 60 mmol) in 70 mL of DMA, under argon. To this was added a solution of 5-amino-2-nitrobenzotrifluoride (12.4 g, 60 mmol) in 80 mL of DMA dropwise, and the mixture was allowed to stir overnight under argon at room temperature. The solvent was removed, and the

residue was diluted with saturated $NaHCO_3$ and extracted with three portions of ethyl acetate. The combined extracts were dried ($MgSO_4$), evaporated, and chromatographed on a silica gel column using dichloromethane as the mobile phase giving 21 g of (*R*)-**3** (80%) (R_f = 0.18, silica gel, CH_2Cl_2): mp 100−101.5 °C; $[\alpha]_D^{25}$ − 44.05 (*c* = 1, MeOH); ^{1}H NMR (DMSO-d_6) δ 10.56 (s, 1H, NH), 8.54 (d, *J* = 2.1 Hz, 1H, ArH), 8.34 (dd, *J* = 9.0 Hz, *J* = 2.1 Hz, 1H, ArH), 8.18 (d, *J* = 9.0 Hz, 1H, ArH), 6.38 (s, 1H, OH), 3.82 (d, *J* = 10.4 Hz, 1H, CH(1)), 3.58 (d, *J* = 10.4 Hz, 1H, CH(2)), 1.48 (s, 3H, Me). Anal. ($C_{11}H_{10}BrF_3N_2O_4$) C, H, N.

***N*-[4-Nitro-3-(trifluoromethyl)phenyl]-(2*S*)-3-bromo-2-hydroxy-2-methylpropan Amide (*S*-3)**. Bromoanilide (*S*)-**3** was prepared from 4.5 g (24 mmol) using the same method as the corresponding *R* isomer giving 6.2 g of (*S*)-**3** (70%) (R_f = 0.18, silica gel, CH_2Cl_2): mp 101.5−102 °C; $[\alpha]_D^{25}$ + 43.90 (*c* = 1, MeOH); ^{1}H NMR (DMSO-d_6) δ 10.55 (s, 1H, NH), 8.54 (d, *J* = 2.3 Hz, 1H, ArH), 8.34 (dd, *J* = 9.0 Hz, *J* = 2.3 Hz, 1H, ArH), 8.18 (d, *J* = 9.0 Hz, 1H, ArH), 6.39 (s, 1H, OH), 3.81 (d, *J* = 10.4 Hz, 1H, CH(1)), 3.57 (d, *J* = 10.4 Hz, 1H, CH(2)), 1.48 (s, 3H, Me). Anal. ($C_{11}H_{10}BrF_3N_2O_4$) C, H, N.

***N*-[4-Amino-3-(trifluoromethyl)phenyl]-(2*R*)-3-bromo-2-hydroxy-2-methylpropan Amide (*R*-4)**. Tin chloride (0.759 g, 10 mmol) was dissolved in 10 mL of methanol and 3 mL of concentrated HCL and cooled to −10 °C. A solution of (*R*)-**3** (0.250 g, 2.0 mmol) in 12 mL of methanol was added in one portion. The reaction mixture was allowed to warm to room temperature and stirred until the reaction was complete as determined by TLC. The reaction mixture was diluted with saturated $NaHCO_3$ and extracted with three 50 mL portions of ethyl acetate. The combined extracts were dried over magnesium sulfate and evaporated to give 0.5 g of a thick amber colored oil (74%): $[\alpha]_D^{25}$ −81.0 (*c* = 2, MeOH); ^{1}H NMR (DMSO-d_6) δ 9.52 (s, 1H, NH), 7.84 (d, *J* = 2.3 Hz, 1H, ArH), 7.55 (dd, *J* = 8.8 Hz, *J* = 2.3 Hz, 1H, ArH), 6.77 (d, *J* = 8.8 Hz, 1H, ArH), 6.09 (s, 1H, OH), 5.39 (s, 2H, NH_2), 3.79 (d, *J* = 10.2 Hz, 1H, CH(1)) 3.55 (d, *J* = 10.2 Hz, 1H, CH(2)), 1.43 (s, 3H, Me). Anal. Calcd for ($C_{11}H_{12}BrF_3N_2O_2$): C, 38.73; H, 3.55; N, 8.21. Found: C, 39.54; H, 3.74; N, 7.81. By NMR the impurity is ethyl acetate and composes 13% of the oil. When this percent of ethyl acetate is accounted for in the elemental analysis, the resulting theoretical and found values are within 0.26% of each other. This oil is so thick that extensive drying under high vacuum was unsuccessful at removing the solvent. MS: [M + H] *m*/*z* 491. MS/MS: *m*/*z* 177 [*p*-amino-*m*-trifluoromethyl-aniline + H].

2-Methyl-oxirane-2-carboxylic Acid (4-Nitro-3-trifluoromethyl-phenyl)-amide (*S*-5). (*R*)-**3** (1.39 g, 3.75 mmol) was dissolved in 50 mL of acetone to which potassium carbonate (1.03 g, 7.49 mmol) was added and stirred at room temperature for 3 h. The solution was diluted with 150 mL of water and extracted with three 100 mL portions of ether. The combined extracts were dried over magnesium sulfate and evaporated giving a yellow colored oil. This oil was a mixture of (*S*)-**5** and 5-amino-2-nitrobenzotrifluoride which was separated on a silica gel column using EtOAc:hexanes (30:70) as the mobile phase giving 0.70 g (2.4 mmol) of (*S*)-**5** as a yellow crystals (64%): mp 83−85 °C; $[\alpha]_D^{26}$ −42.1; ^{1}H NMR (DMSO-d_6) δ 10.26 (s, 1H, NH), 8.41 (d, *J* = 2.09 Hz, 1H, ArH), 8.26 (dd, *J* = 9.0 Hz, *J* = 2.2 Hz, 1H, ArH), 8.18 (d, *J* = 9.0 Hz, 1H, ArH), 3.08 (d, *J* = 5.2 Hz, 1H, CH(1)) 3.14 (d, *J* = 5.2 Hz, 1H, CH(2)), 1.47 (s, 3H, Me). Anal. ($C_{11}H_9F_3N_2O_4$) C, H, N.

Androgen Receptor Competitive Binding Assay. AR binding affinities of the synthesized ligands were determined by the competitive binding assay as described previously.[36]

FlexX Docking and Complex Refinement. Docking was performed with FlexX[57,58] using the SYBYL 6.5[52] as a front end. FlexX performs flexible docking using an incremental fragment construction method to place a flexible ligand into a rigid protein structure. To prepare the AR G1 model for docking, all hydrogens were removed, and the ligand binding site was defined as all residues within 6.5 Å of TES. Ligands were docked into the ligand binding site with hydrogens present, and formal charges were assigned to the nitro group. Although no charge is assigned to the nitro group, this descriptor is used for identifying interaction types that apply to the nitro group (i.e., salt bridge interactions). The top 30 scoring docking solutions were saved. All energy minimization and MD simulations were performed with the AMBER 5[37] suite of programs using the "parm99" parameters.[42] The ligand was minimized within the complex to an RMS gradient of 0.001 kcal/Å, while restraining the protein atoms to their initial positions with a harmonic potential of 100 kcal/Å^2, to remove bad contacts which result from the use of two different energy functions in the different stages (i.e., initial docking and refinement). Another 2000 steps of minimization were performed while restraining the protein backbone atoms to their initial positions with a harmonic potential of 50 kcal/Å^2. Both minimization steps used an 8 Å residue charge group based cutoff with a distance dependent dielectric of 4*r*. All MD simulations use an 8 Å residue charge group based cutoff for nonbonded interactions, a dielectric constant of 1, Berendsen coupling for constant temperature,[59] SHAKE[60] to constrain bonds to hydrogen, and a 1.5 fs time step. The minimized protein ligand complex was then solvated in a 40 Å cap of TIP3P waters followed by a 1000-step minimization of the water molecules while holding the protein atoms to their initial positions with a harmonic potential of 5 kcal/Å^2. A 50 ps belly MD equilibration of only the water was performed at 300 K. The complex was then warmed from 0 to 300 K over 25 ps followed by an equilibration period of 25 ps at 300 K with a 0.5 kcal/Å^2 harmonic positional restraint on the protein. The final step of complex refinement was a 150 ps belly MD simulation of the ligand, and all residues within a 12 Å radius around the ligand at 300 K. The trajectories were averaged once the potential energy reached a stable value, typically within 10 ps or less, followed by minimization of the average structure for 5000 steps.

Acknowledgment. We express our gratitude to Dr. Pedro Matias at the Instituto de Tecnologia Quimica e Biologica, Universidade Nova de Lisboa, for performing the RMSD comparison calculations and general comments on the model; Dr. Junmei Wang and Dr. Peter Kollman at University of California San Fransisco for making available the *parmscan* program and the parm99 parameters prior to publication; and Dr. Henry Kurtz at the University of Memphis for his help with ab initio calculations on TES and PGT. Funding for this work was provided by the U.T. College of Pharmacy, the Van Vleet Foundation, the St. Francis of Assisi Foundation, and grants from the National Cancer Institute (R29 CA 68096-0) and the National Institute of Diabetes and Digestive Kidney Disease (R01-DK59800-01).

Supporting Information Available: A table with the hPR control simulation results and tables with AMBER force field parameters for the TES, PGT, and nonsteroidal ligand are presented. This material is available free of charge via the Internet at http://pubs.acs.org. Pdb files with the atomic coordinates for the G1 and G2 models are available upon request.

References

(1) Evans, R. M. The Steroid and Thyroid Hormone Receptor Superfamily. *Science* **1988**, *240*, 889−894.
(2) Rosen, J.; Day, A.; Jones, T. K.; Jones, E. T.; Nadzan, A. M.; Stein, R. B. Intracellular receptors and signal transducers and activators of transcription superfamilies: novel targets for small-molecule drug discovery. *J. Med. Chem.* **1995**, *38*, 4855−74.
(3) Matsumoto, A. M. Hormonal therapy of male hypogonadism. *Endocrinol. Metab. Clin. North Am.* **1994**, *23*, 857−75.
(4) Wurtz, J. M.; Bourguet, W.; Renaud, J. P.; Vivat, V.; Chambon, P.; Moras, D.; Gronemeyer, H. A canonical structure for the ligand-binding domain of nuclear receptors. *Nat. Struct. Biol.* **1996**, *3*, 206.
(5) Wagner, R. L.; Apriletti, J. W.; McGrath, M. E.; West, B. L.; Baxter, J. D.; Fletterick, R. J. A structural role for hormone in the thyroid hormone receptor. *Nature* **1995**, *378*, 690−7.

(6) Brzozowski, A. M.; Pike, A. C.; Dauter, Z.; Hubbard, R. E.; Bonn, T.; Engstrom, O.; Ohman, L.; Greene, G. L.; Gustafsson, J. A.; Carlquist, M. Molecular basis of agonism and antagonism in the oestrogen receptor. *Nature* **1997**, *389*, 753−8.
(7) Tanenbaum, D. M.; Wang, Y.; Williams, S. P.; Sigler, P. B. Crystallographic comparison of the estrogen and progesterone receptor's ligand binding domains. *Proc. Natl. Acad. Sci. U.S.A.* **1998**, *95*, 5998−6003.
(8) Williams, S. P.; Sigler, P. B. Atomic structure of progesterone complexed with its receptor. *Nature* **1998**, *393*, 392−6.
(9) Nolte, R. T.; Wisely, G. B.; Westin, S.; Cobb, J. E.; Lambert, M. H.; Kurokawa, R.; Rosenfeld, M. G.; Willson, T. M.; Glass, C. K.; Milburn, M. V. Ligand binding and co-activator assembly of the peroxisome proliferator-activated receptor-gamma. *Nature* **1998**, *395*, 137−43.
(10) Xu, H. E.; Lambert, M. H.; Montana, V. G.; Parks, D. J.; Blanchard, S. G.; Brown, P. J.; Sternbach, D. D.; Lehmann, J. M.; Wisely, G. B.; Willson, T. M.; Kliewer, S. A.; Milburn, M. V. Molecular recognition of fatty acids by peroxisome proliferator-activated receptors. *Mol. Cell* **1999**, *3*, 397−403.
(11) Rochel, N.; Wurtz, J. M.; Mitschler, A.; Klaholz, B.; Moras, D. The crystal structure of the nuclear receptor for vitamin D bound to its natural ligand. *Mol. Cell* **2000**, *5*, 173−9.
(12) Matias, P. M.; Donner, P.; Coelho, R.; Thomaz, M.; Peixoto, C.; Macedo, S.; Otto, N.; Joschko, S.; Scholz, P.; Wegg, A.; Basler, S.; Schafer, M.; Ruff, M.; Egner, U.; Carrondo, M. A. Structural evidence for ligand specificity in the binding domain of the human Androgen receptor: implications for pathogenic gene mutations. *J. Biol. Chem.* **2000**, *275*, 26164−26171.
(13) Furr, B. J. A.; Tucker, H. The Preclinical Development of Bicalutamide: Pharmacodynamics and Mechanism of Action. *Urology* **1996**, *47*, 13−25.
(14) Morris, J. J.; Hughes, L. R.; Glen, A. T.; Taylor, P. J. Nonsteroidal antiandrogens. Design of novel compounds based on an infrared study of the dominant conformation and hydrogen-bonding properties of a series of anilide antiandrogens. *J. Med. Chem.* **1991**, *34*, 447−55.
(15) Mukherjee, A.; Kirkovsky, L.; Yao, X. T.; Yates, R. C.; Miller, D. D.; Dalton, J. T. Enantioselective binding of Casodex to the androgen receptor. *Xenobiotica* **1996**, *26*, 117−22.
(16) Caves, L. S.; Evanseck, J. D.; Karplus, M. Locally accessible conformations of proteins: multiple molecular dynamics simulations of crambin. *Protein Sci.* **1998**, *7*, 649−66.
(17) Colombo, G.; Merz, K. M., Jr. Stability and Activity of Mesophilic Subtilisin E and Its Thermophilic Homolog: Insights from Molecular Dynamics Simulations. *J. Am. Chem. Soc.* **1999**, *121*, 6895−6903.
(18) York, D. M.; Darden, T. A.; Pedersen, L. G.; Anderson, M. W. Molecular dynamics simulation of HIV-1 protease in a crystalline environment and in solution. *Biochemistry* **1993**, *32*, 1443−53.
(19) Langley, E.; Kemppainen, J. A.; Wilson, E. M. Intermolecular NH2-/carboxyl-terminal interactions in androgen receptor dimerization revealed by mutations that cause androgen insensitivity. *J. Biol. Chem.* **1998**, *273*, 92−101.
(20) Singh, S. M.; Gauthier, S.; Labrie, F. Androgen receptor antagonists (antiandrogens): structure−activity relationships. *Curr. Med. Chem.* **2000**, *7*, 211−47.
(21) Ferrin, T. E.; Huang, C. C.; Jarvis, L. E.; Langridge, R. The MIDAS display system. *J. Mol. Graphics* **1988**, *6*, 13−27.
(22) Huang, C. C.; Pettersen, E. F.; Klein, T. E.; Ferrin, T. E.; Langridge, R. CONIC: A fast renderer for space-filling molecules with shadows. *J. Mol. Graphics* **1991**, *9*, 230−236.
(23) Laskowski, R. A.; MacArthur, M. W.; Moss, D. S.; Thornton, J. M. PROCHECK: a program to check the stereochemical quality of protein structures. *J. Appl. Crystallogr.* **1993**, *26*, 283−291.
(24) De Bellis, A.; Quigley, C. A.; Cariello, N. F.; el-Awady, M. K.; Sar, M.; Lane, M. V.; Wilson, E. M.; French, F. S. Single base mutations in the human androgen receptor gene causing complete androgen insensitivity: rapid detection by a modified denaturing gradient gel electrophoresis technique. *Mol. Endocrinol.* **1992**, *6*, 1909−20.
(25) Lumbroso, S.; Lobaccaro, J. M.; Georget, V.; Leger, J.; Poujol, N.; Terouanne, B.; Evain-Brion, D.; Czernichow, P.; Sultan, C. A novel substitution (Leu707Arg) in exon 4 of the androgen receptor gene causes complete androgen resistance. *J. Clin. Endocrinol. Metab.* **1996**, *81*, 1984−8.
(26) Marcelli, M.; Zoppi, S.; Wilson, C. M.; Griffin, J. E.; McPhaul, M. J. Amino acid substitutions in the hormone-binding domain of the human androgen receptor alter the stability of the hormone receptor complex. *J. Clin. Invest.* **1994**, *94*, 1642−50.
(27) Bevan, C. L.; Brown, B. B.; Davies, H. R.; Evans, B. A.; Hughes, I. A.; Patterson, M. N. Functional analysis of six androgen receptor mutations identified in patients with partial androgen insensitivity syndrome. *Hum Mol Genet* **1996**, *5*, 265−73.
(28) Batch, J. A.; Williams, D. M.; Davies, H. R.; Brown, B. D.; Evans, B. A.; Hughes, I. A.; Patterson, M. N. Androgen receptor gene mutations identified by SSCP in fourteen subjects with androgen insensitivity syndrome. *Hum. Mol. Genet.* **1992**, *1*, 497−503.
(29) Ris-Stalpers, C.; Hoogenboezem, T.; Sleddens, H. F.; Verleun-Mooijman, M. C.; Degenhart, H. J.; Drop, S. L.; Halley, D. J.; Oosterwijk, J. C.; Hodgins, M. B.; Trapman, J.; et al. A practical approach to the detection of androgen receptor gene mutations and pedigree analysis in families with x-linked androgen insensitivity. *Pediatr. Res.* **1994**, *36*, 227−34.
(30) Nakao, R.; Haji, M.; Yanase, T.; Ogo, A.; Takayanagi, R.; Katsube, T.; Fukumaki, Y.; Nawata, H. A single amino acid substitution (Met786_Val) in the steroid-binding domain of human androgen receptor leads to complete androgen insensitivity syndrome. *J. Clin. Endocrinol. Metab.* **1992**, *74*, 1152−7.
(31) Veldscholte, J.; Ris-Stalpers, C.; Kuiper, G. G.; Jenster, G.; Berrevoets, C.; Claassen, E.; van Rooij, H. C.; Trapman, J.; Brinkmann, A. O.; Mulder, E. A mutation in the ligand binding domain of the androgen receptor of human LNCaP cells affects steroid binding characteristics and response to anti-androgens. *Biochem. Biophys. Res. Commun.* **1990**, *173*, 534−40.
(32) De Bellis, A.; Quigley, C. A.; Marschke, K. B.; el-Awady, M. K.; Lane, M. V.; Smith, E. P.; Sar, M.; Wilson, E. M.; French, F. S. Characterization of mutant androgen receptors causing partial androgen insensitivity syndrome. *J. Clin. Endocrinol. Metab.* **1994**, *78*, 513−22.
(33) Lundberg Giwercman, Y.; Nikoshkov, A.; Lindsten, K.; Bystrom, B.; Pousette, A.; Chibalin, A. V.; Arvidsson, S.; Tiulpakov, A.; Semitcheva, T. V.; Peterkova, V.; Hagenfeldt, K.; Ritzen, E. M.; Wedell, A. Functional characterisation of mutations in the ligand-binding domain of the androgen receptor gene in patients with androgen insensitivity syndrome. *Hum. Genet.* **1998**, *103*, 529−31.
(34) Letz, M.; Bringmann, P.; Mann, M.; Mueller-Fahrnow, A.; Reipert, D.; Scholz, P.; Wurtz, J. M.; Egner, U. Investigation of the binding interactions of progesterone using muteins of the human progesterone receptor ligand binding domain designed on the basis of a three-dimensional protein model. *Biochim. Biophys. Acta* **1999**, *1429*, 391−400.
(35) Poujol, N.; Wurtz, J. M.; Tahiri, B.; Lumbroso, S.; Nicolas, J. C.; Moras, D.; Sultan, C. Specific recognition of androgens by their nuclear receptor: a structure−function study. *J. Biol. Chem.* **2000**, *275*, 24022−24031.
(36) Kirkovsky, L.; Mukherjee, A.; Yin, D.; Dalton, J. T.; Miller, D. D. Chiral nonsteroidal affinity ligands for the androgen receptor. 1. Bicalutamide analogues bearing electrophilic groups in the B aromatic ring. *J. Med. Chem.* **2000**, *43*, 581−90.
(37) Case, D. A.; Pearlman, D. A.; Cladwell, J. W.; Cheatham, T. E., III; Ross, W. S.; Simmerling, C. L.; Darden, T. A.; Merz, K. M.; Stanton, R. V.; Cheng, A. L.; Vincent, J. J.; Crowley, M.; Ferguson, D. M.; Radmer, R. J.; Seibel, G. L.; Singh, U. C.; Weiner, P. K.; Kollman, P. A. AMBER 5; University of California: San Francisco, 1997.
(38) Cornell, W. D.; Cieplak, P.; Bayly, C. I.; Gould, I. R.; Merz Jr., K. M.; Ferguson, D. M.; Spellmeyer, D. C.; Fox, T.; Caldwell, J. W.; Kollman, P. A. A Second Generation Force Field for the Simulation of Proteins, Nucleic Acids, and Organic Molecules. *J. Am. Chem. Soc.* **1995**, *117*, 5179−5197.
(39) Bayly, C. I.; Cieplak, P.; Cornell, W. D.; Kollman, P. A. A Well-Behaved Electrostatic Potential Based Method Using Charge Restraints For Determining Atom-Centered Charges: The RESP Model. *J. Phys. Chem.* **1993**, *97*, 10269−10280.
(40) Cieplak, P.; Cornell, W. D.; Bayly, C.; Kollman, P. A. Applications of the Multimolecule and Multiconformational RESP Methodology to Biopolymers: Charge Derivation for DNA, RNA, and Proteins. *J. Comput. Chem.* **1995**, *16*, 1357−1377.
(41) Frisch, M. J.; Trucks, G. W.; Schlegel, H. B.; Scuseria, G. E.; Robb, M. A.; Cheeseman, J. R.; Zakrzewski, V. G.; Montgomery, J. A.; Stratmann, R. E.; Burant, J. C.; Dapprich, S.; Millam, J. M.; Daniels, A. D.; Kudin, K. N.; Strain, M. C.; Farkas, O.; Tomasi, J.; Barone, V.; Cossi, M.; Cammi, R.; Mennucci, B.; Pomelli, C.; Adamo, C.; Clifford, S.; Ochterski, J.; Petersson, G. A.; Ayala, P. Y.; Cui, Q.; Morokuma, K.; Malick, D. K.; Rabuck, A. D.; Raghavachari, K.; Foresman, J. B.; Cioslowski, J.; Ortiz, J. V.; Stefanov, B. B.; Liu, G.; Liashenko, A.; Piskorz, P.; Komaromi, I.; Gomperts, R.; Martin, R. L.; Fox, D. J.; Keith, T.; Al-Laham, M. A.; Peng, C. Y.; Nanayakkara, A.; Gonzalez, C.; Challacombe, M.; Gill, P. M. W.; Johnson, B. G.; Chen, W.; Wong, M. W.; Andres, J. L.; Head-Gordon, M.; Replogle, E. S.; Pople, J. A. Gaussian 98 (Revision A.9); Gaussian, Inc: Pittsburgh, PA, 1998.
(42) Wang, J.; Cieplak, P.; Kollman, P. A. How well does a restrained electrostatic potential (RESP) model perform in calculating conformational energies of organic and biological molecules? *J. Comput. Chem.* **2000**, *21*, 1049−1074.
(43) Labaree, D. C.; Hoyte, R. M.; Nazareth, L. V.; Weigel, N. L.; Hochberg, R. B. 7alpha-Iodo and 7alpha-fluoro steroids as androgen receptor-mediated imaging agents. *J. Med. Chem.* **1999**, *42*, 2021−34.

(44) Glen, A. T.; Hughes, L. R.; Morris, J. J.; Taylor, P. T. *Structure−activity Relationships Among Nonsteroidal antiandrogens*; Lambert, R. W., Ed.; Royal Society of Chemistry: London, 1986; pp 345−361.
(45) Van Dort, M. E.; Robins, D. M.; Wayburn, B. Design, synthesis, and pharmacological characterization of 4-[4, 4-dimethyl-3-(4-hydroxybutyl)-5-oxo-2-thioxo-1-imidazolidinyl]-2-iodobenzonitrile as a high-affinity nonsteroidal androgen receptor ligand. *J. Med. Chem.* **2000**, *43*, 3344−7.
(46) Tucker, H.; Crook, J. W.; Chesterson, G. J. Nonsteroidal antiandrogens. Synthesis and structure−activity relationships of 3-substituted derivatives of 2-hydroxypropionanilides. *J. Med. Chem.* **1988**, *31*, 954−9.
(47) Dukes M, F. B., Hughes LR, Tucker H, Woodburn JR Nonsteroidal progestins and antiprogestins related to flutamide. *Steroids* **2000**, *65*, 725−731.
(48) Teutsch, G.; Goubet, F.; Battmann, T.; Bonfils, A.; Bouchoux, F.; Cerede, E.; Gofflo, D.; Gaillard-Kelly, M.; Philibert, D. Nonsteroidal antiandrogens: synthesis and biological profile of high-affinity ligands for the androgen receptor. *J. Steroid Biochem. Mol. Biol.* **1994**, *48*, 111−9.
(49) Ojasoo, T.; Delettre, J.; Mornon, J. P.; Turpin-VanDycke, C.; Raynaud, J. P. Towards the mapping of the progesterone and androgen receptors. *J. Steroid Biochem.* **1987**, *27*, 255−69.
(50) Dalton, J. T.; Mukherjee, A.; Zhu, Z.; Kirkovsky, L.; Miller, D. D. Discovery of nonsteroidal androgens. *Biochem. Biophys. Res. Commun.* **1998**, *244*, 1−4.
(51) Wakeling, A. E.; Furr, B. J.; Glen, A. T.; Hughes, L. R. Receptor binding and biological activity of steroidal and nonsteroidal antiandrogens. *J. Steroid Biochem.* **1981**, *15*, 355−9.
(52) Tripos Associates, 1699 South Hanley Rd., Suite 303, St. Louis, MO 63144.
(53) Fox, T.; Kollman, P. A. The application of different solvation and electrostatic models in molecular dynamics simulations of ubiquitin: how well is the X-ray structure "maintained"? *Proteins* **1996**, *25*, 315−34.
(54) Ryckaert, J. P.; Ciccotti, G.; Berendsen, H. J. C. Numerical intergration of the Cartesian equations of motion of a system with constraints: molecular dynamics of *n*-alkanes. *J. Comput. Phys.* **1977**, *23*, 327−341.
(55) Schreiber, H.; Steinhauser, O. Cutoff size does strongly influence molecular dynamics results on solvated polypeptides. *Biochemistry* **1992**, *31*, 5856−60.
(56) Tucker, H.; Chesterson, G. J. Resolution of the nonsteroidal antiandrogen 4′-cyano-3-[(4-fluorophenyl)sulfonyl]-2-hydroxy-2-methyl-3′- (trifluoromethyl)-propionanilide and the determination of the absolute configuration of the active enantiomer. *J. Med. Chem.* **1988**, *31*, 885−7.
(57) Rarey, M.; Kramer, B.; Lengauer, T.; Klebe, G. A fast flexible docking method using an incremental construction algorithm. *J. Mol. Biol.* **1996**, *261*, 470−89.
(58) Kramer, B.; Rarey, M.; Lengauer, T. Evaluation of the FLEXX incremental construction algorithm for protein−ligand docking. *Proteins* **1999**, *37*, 228−41.
(59) Berendsen, H. J. C.; Postma, J. P. M.; vanGunsteren, W. F.; DiNola, A.; Haak, J. R. Molecular dynamics with coupling to an external bath. *J. Comput. Phys.* **1984**, *81*, 3684−3690.
(60) Ryckaert, J. P.; Ciccotti, G.; Berendsen, H. J. C. Numerical integration of the Cartesian equations of motion of a system with consraints: molecular dynamics of *n*-alkanes. *J. Comput. Phys.* **1977**, *23*, 327−341.

JM0005353